International Journal of Biochemistry and Cell Biology 114 (2019) 105573

Contents lists available at ScienceDirect

International Journal of Biochemistry and Cell Biology

journal homepage: www.elsevier.com/locate/biocel

Maduramicin inactivation of Akt impairs autophagic flux leading to accumulated autophagosomes-dependent apoptosis in skeletal myoblast cells

Xiaoqing Dong[a,1], Rui Zhao[a,1], Yue Li[a,1], Qianyun Yu[a], Xin Chen[a], Xiaoyu Hu[a], Jing Ma[a], Xiaoling Chen[a], Shile Huang[b,c,**], Long Chen[a,*]

[a] Jiangsu Key Laboratory for Molecular and Medical Biotechnology, College of Life Sciences, Nanjing Normal University, Nanjing 210023, PR China
[b] Department of Biochemistry and Molecular Biology, Louisiana State University Health Sciences Center, Shreveport, LA 71130-3932, USA
[c] Feist-Weiller Cancer Center, Louisiana State University Health Sciences Center, Shreveport, LA 71130-3932, USA

ARTICLE INFO

Keywords:
Maduramicin
Apoptosis
Autophagosome
Akt
Autophagic flux

ABSTRACT

It has been clinically documented that maduramicin (Mad), a polyether ionophore antibiotic widely used in the control of coccidiosis in poultry worldwide, can elicit skeletal muscle degeneration, heart failure, and even death in animals and humans, if improperly used. Here, we show that Mad induced apoptosis dose-dependently, which was associated with impaired autophagic flux in skeletal myoblast (C2C12 and L6) cells. This is supported by the findings that Mad treatment resulted in increase of autophagosomes with a concomitant elevation of LC3-II and p62 in the cells. Also, Mad increased co-localization of mCherry and GFP tandem-tagged LC3 puncta in the cells, suggesting a blockage of autophagic flux. Furthermore, addition of chloroquine (CQ) strengthened the basic and Mad-enhanced LC3-II and p62 levels, autophagosome formation and cell apoptosis, whereas pretreatment with rapamycin alleviated the effects in the cells exposed to Mad. Moreover, we noticed that Mad treatment inactivated Akt dose-dependently. Inhibition of Akt with inhibitor X potentiated Mad-induced decrease in phosphorylated Akt, and increases in LC3-II and p62 levels, autophagosome formation and cell apoptosis, whereas ectopic expression of constitutively active Akt rendered resistance to these events. Collectively, these results indicate that Mad inactivation of Akt impairs autophagic flux leading to accumulated autophagosomes-dependent apoptosis in skeletal myoblast cells. Our findings suggest that manipulation of Akt activity to improve autophagic flux is a promising strategy against Mad-induced myotoxicity.

1. Introduction

Maduramicin (Mad) is a monovalent glycoside polyether ionophore antibiotic, produced by aerobic fermentation of *Actinomadura yumaensis* bacteria originally isolated from soil samples in Yuma County, Arizona, USA (Liu et al., 1983). It was first used to control coccidiosis in poultry (Dorne et al., 2013; Liu et al., 1983). The safe dose of Mad is 5 mg/kg, which is comparable to the efficacy of monensin against coccidiosis of 120 mg/kg (Dorne et al., 2013; Singh and Gupta, 2003). However, when the dose increases to 7–9 mg/kg, Mad can cause broiler poisoning (Singh and Gupta, 2003), suggesting that Mad has a very narrow safe dose range and very strong toxicity. Chickens and turkeys discharge Mad prototypes, causing environmental pollution (Gutierrez-Lugo et al., 1999). Moreover, extensive use of Mad on farms may lead to residues in livestock and some ruminants (Kozarova et al., 2011; Olejnik et al., 2013, 2011; Rokka et al., 2005; Spisso et al., 2010). When a human consumes Mad-contaminated food, Mad can be excreted in the feces. However, studies have shown that Mad cannot be excreted completely, and some residual Mad remains in the human body (Wang et al., 2008). Mad poisoning, such as rhabdomyolysis, skeletal muscle

Abbreviations: Akt, protein kinase B (PKB); CQ, chloroquine; DAPI, 4′6-diamidino-2-phenylindole; DMEM, Dulbecco's Modified Eagle's Medium; FBS, fetal bovine serum; GSK3β, glycogen synthase kinase3β; LC3, microtuble-associated protein 1 light chain 3; Mad, maduramicin; MDC, monodansylcadaverine; PBS, phosphate buffered saline; TUNEL, terminal deoxynucleotidyl transferase (TdT)-mediated deoxyuridine triphosphate (dUTP) nick-end labeling

* Corresponding author at: College of Life Sciences, Nanjing Normal University, 1 Wenyuan Road, Chixia District, Nanjing 210023, Jiangsu, PR China.
** Corresponding author at: Department of Biochemistry and Molecular Biology, Louisiana State University Health Sciences Center, 1501 Kings Highway, Shreveport, LA 71130-3932, USA.
E-mail addresses: shuan1@lsuhsc.edu (S. Huang), lchen@njnu.edu.cn (L. Chen).
[1] These authors contributed equally to this work.

https://doi.org/10.1016/j.biocel.2019.105573
Received 20 January 2019; Received in revised form 17 June 2019; Accepted 16 July 2019
Available online 17 July 2019

degeneration, heart failure, and even death, has been documented in humans (Jayashree and Singhi, 2011; Sharma et al., 2005). However, how Mad induces myotoxicity is not well understood.

Autophagy, as one of the major pathways for protein degradation, is a multistep process involving the formation of double-membrane autophagosomes that engulf cytosolic components and deliver cargo to lysosomes for digestion and nutrient recycling (Bruntz et al., 2014; Mizushima and Klionsky, 2007; Mizushima et al., 2008). Overwhelming evidence has demonstrated that autophagy is required for the development, differentiation, tissue remodeling, and immune regulation of various organisms (Deretic et al., 2013; Levine and Klionsky, 2004; Levine and Kroemer, 2008; Mizushima and Levine, 2010). So, autophagic dysfunction or impaired autophagic degradation is associated with the pathogenesis of many human diseases including infections, cancer, neurodegeneration, aging, heart disease, and muscle disease (Levine and Kroemer, 2008; Mizushima et al., 2008). The microtubule-associated protein 1 light chain 3 (LC3) includes two molecular forms, LC3-I and LC3-II. LC3-I is the unconjugated form in the cytosol, whereas LC3-II is the conjugated form that binds to autophagosomes and directly correlates with the number of autophagosomes (Kabeya et al., 2000; Ni et al., 2011). Thus, the manifestation of LC3-II or GFP-LC3-II is considered as a marker for monitoring the status of autophagy. However, of note, the overall activity of the autophagy pathway can be robustly measured by autophagic flux (Mizushima et al., 2010). When the function of lysosomes is impaired or autophagosomes cannot fuse with lysosomes to form autolysosomes and the contents of autolysosomes cannot be degraded, the status is called autophagic flux impairment (Yin et al., 2017; Zhang et al., 2013). The p62 protein, also called sequestosome 1 (SQSTM1), is a ubiquitin-binding scaffold protein and itself degraded along with its cargo by autophagy (Yin et al., 2017; Zhang et al., 2013). Inhibition of autophagy is associated with a lessened p62 degradation leading to p62 accumulation in the cytosol (Zhang et al., 2013). In contrast, intact autophagic flux promotes p62 degradation, showing decreased p62 protein level in the cells (Zhang et al., 2013). Our group has recently shown that Mad inhibits autophagic flux involved in apoptosis in myocardial H9c2 cells (Chen et al., 2018). This prompts us to explore and clarify the relationship between autophagy and apoptosis in skeletal myoblast cells induced by Mad, as well as the underlying mechanisms.

Protein kinase B (PKB, also known as Akt), a serine/threonine protein kinase, plays a critical role in the regulation of cell survival (Degtyarev et al., 2008; Dudek et al., 1997). Akt inactivation is necessary for the autophagic process (Arico et al., 2001; Bruntz et al., 2014; Degtyarev et al., 2008; Kuo et al., 2006). For example, inactivation of Akt leads to cell viability reduction and death in glioblastoma cells by specifically inhibiting autophagic flux (Bruntz et al., 2014). The dephosphorylation of Akt at Thr308 and Ser473 is associated with the reduction of autophagic flux and an additional upregulation of caspase-3 activity in liver cancer cells in response to sorafenib (Rodriguez-Hernandez et al., 2018). Here, for the first time, we show that Mad inactivation of Akt impairs autophagic flux leading to accumulated autophagosomes-dependent apoptosis in skeletal myoblast (C2C12 and L6) cells. Our findings suggest that manipulation of Akt activity to improve autophagic flux may be a promising strategy against Mad-induced myotoxicity.

2. Materials and methods

2.1. Materials

Maduramicin ammonium and Akt inhibitor X were provided by Santa Cruz Biotechnology (Santa Cruz, CA, USA), whereas chloroquine diphosphate (CQ), monodansylcadaverine (MDC), 4′,6-diamidino-2-phenylindole (DAPI) and protease inhibitor cocktail were purchased from Sigma (St Louis, MO, USA). Rapamycin were from ALEXIS Biochemicals Corporation (San Diego, CA, USA). Dulbecco's modified Eagle medium (DMEM) and 0.05% Trypsin-EDTA were purchased from Invitrogen (Grand Island, NY, USA). Fetal bovine serum (FBS) was supplied by Hyclone (Logan, UT, USA). Enhanced chemiluminescence solution was from Sciben Biotech Company (Nanjing, China). Other chemicals were purchased from local commercial sources and were of analytical grade.

2.2. Cell culture

Mouse C2C12 myoblast cells (C2C12 cells) (#CRL-1772) and rat L6 myoblast cells (L6 cells) (#CRL-1458) were obtained from American Type Culture Collection (Manassas, VA, USA). For culture, cells, seeded in a 6-well or 96-well plate, were maintained in 4.5 mg/ml high glucose DMEM supplemented with 10% FBS, 100 U/ml penicillin, 100 U/ml streptomycin and 2 mM L-glutamine, and incubated at 37 °C in a humidified incubator containing 5% CO_2.

2.3. Recombinant adenoviral constructs and infection of cells

Recombinant adenoviral vector encoding HA-tagged constitutively active Akt (Ad-myr-Akt) was generously provided by Dr. Kenneth Walsh (Boston University, Boston, MA), and the control virus expressing β-galactosidase (Ad-LacZ) was described previously (Liu et al., 2010). Adenoviruses expressing GFP-tagged LC3 fusion protein (Ad-GFP-LC3), GFP-tagged p62 fusion protein (Ad-GFP-p62), and mCherry-GFP tandem-tagged LC3 fusion protein (Ad-mCherry-GFP-LC3) were purchased from Sciben Biotech Company (Nanjing, China). For experiments, C2C12 and L6 cells were grown in the growth medium and infected with the individual adenovirus for 24 h at 5 of multiplicity of infection (MOI = 5). Subsequently, the infected cells were used for further experiments. Ad-LacZ served as a control. Expression of HA-tagged myr-Akt was determined by Western blotting with an antibody to HA.

2.4. Analysis for cell viability

C2C12 and L6 cells, or C2C12 cells infected with Ad-myr-Akt or Ad-LacZ, respectively, were seeded in a 96-well plate (1×10^4 cells/well). The next day, cells were treated with/without Mad (0.5 and 1 μM) for 24 h, or with/without Mad (0.5 and 1 μM) for 24 h following pretreatment with/without Akt inhibitor X (10 μM) for 2 h, with 5 replicates of each treatment. Subsequently, cell viability, after incubation with MTS reagent (one solution reagent) (20 μl/well) for 3 h, was evaluated by measuring the optical density (OD) at 490 nm using a Victor X3 Light Plate Reader (PerkinElmer, Waltham, MA, USA).

2.5. MDC-labeled autophagic vacuoles

Intracellular autophagic status was evaluated using a selective marker MDC for autophagic vacuoles, as described (Biederbick et al., 1995; Munafo and Colombo, 2001). In brief, C2C12 and L6 cells were seeded at a density of 5×10^5 cells/well in a 6-well plate containing a glass coverslip per well. The next day, cells were treated with/without Mad (0.05, 0.1, 0.2, 0.5 and 1 μM) for 24 h, or treated with/without Mad (0.5 and 1 μM) for 24 h following pretreatment with/without CQ (5 μM) for 1 h, with 5 replicates of each treatment. Subsequently, the cells were labeled with 0.05 mM MDC in PBS for 10 min at 37 °C and then washed 3 times with PBS, followed by cell imaging under a fluorescence microscopy (Leica DMi8, Wetzlar, Germany) equipped with a digital camera. At least five independent fields per well were photographed. For quantitative analysis of the fluorescence intensity for MDC staining, the integral optical density (IOD) was measured by Image-Pro Plus 6.0 software (Media Cybernetics Inc., Newburyport, MA, USA).

2.6. GFP-LC3, GFP-p62 or mCherry-GFP-LC3 assay

C2C12 and L6 cells, or C2C12 cells infected with Ad-myr-Akt or Ad-LacZ, respectively, were infected with Ad-GFP-LC3, Ad-GFP-p62 or Ad-mCherry-GFP-LC3 and seeded at a density of 5×10^5 cells/well in a 6-well plate containing a glass coverslip per well. The next day, cells were treated with/without Mad (0.05, 0.1, 0.2, 0.5 and/or 1 μM) for 24 h, or with/without Mad (0.5 and 1 μM) for 24 h following pretreatment with/without CQ (5 μM) for 1 h, rapamycin (0.2 μg/ml) for 24 h or Akt inhibitor X (10 μM) for 2 h, with 5 replicates of each treatment. Afterwards, the cells were fixed with 4% paraformaldehyde in PBS for 30 min at 4 °C, followed by washing 3 times with PBS. For the cells infected with Ad-mCherry-GFP-LC3, after treatments, the cells were stained with DAPI (4 μg/ml in deionized water) as described (Chen et al., 2008). Finally, photographs were taken under a fluorescence microscopy (Leica DMi8, Wetzlar, Germany) equipped with a digital camera, followed by counting the numbers of GFP-LC3 puncta (green) and GFP-p62 (green) per cell to estimate autophagosome formation and autophagic flux manifestation, respectively. In mCherry-GFP tandem-tagged LC3 assay, autophagosome and autolysome status was evaluated by counting cells with $GFP^+/mCherry^+$ (yellow) puncta. Induction of autophagy causes punctate localization of LC3 on autophagosomes, which exhibits both GFP (green) and mCherry (red) fluorescence (Ma et al., 2012). Because of the different pH stabilities of the green and red fluorescent proteins, the GFP-LC3 loses its fluorescent signal within the acidic intralysosomal environment, but the mCherry-LC3 signal persists (Ma et al., 2012). Therefore, when an autophagosome has not yet fused with a lysosome or when the degradation's function of lysosome with acidification is impaired, co-localization of both GFP and mCherry fluorescence shows $GFP^+/mCherry^+$-LC3 (yellow) puncta, which are indicative of autophagosomes, in the merged image. In contrast, mCherry alone (without GFP) fluorescence presents $GFP^-/mCherry^+$-LC3 (red) puncta, which are indicative of autolysosomes.

2.7. DAPI and TUNEL staining

C2C12 and L6 cells, or C2C12 cells infected with Ad-myr-Akt or Ad-LacZ, respectively, were seeded at a density of 5×10^5 cells/well in a 6-well plate containing a glass coverslip per well. The next day, cells were treated with/without Mad (0.05, 0.1, 0.2, 0.5 and/or 1 μM) for 24 h, or with/without Mad (0.5 and 1 μM) for 24 h following pretreatment with/without CQ (5 μM) for 1 h, rapamycin (0.2 μg/ml) for 24 h or Akt inhibitor X (10 μM) for 2 h, with 5 replicates of each treatment. Subsequently, the cells with fragmented and condensed nuclei were stained with DAPI (4 μg/ml in deionized water) as described (Chen et al., 2008). For the cells exposed to 0–1 μM of Mad for 24 h, after DAPI staining, the following staining was performed by adding terminal deoxynucleotidyl transferase (TdT)-mediated deoxyuridine triphosphate (dUTP) nick-end labeling (TUNEL) reaction mixture (TdT enzyme solution and labeling solution) according to the manufacturer's protocols of *in situ* Cell Death Detection Kit® (Roche, Mannheim, Germany). Finally, photographs were taken under a fluorescence microscope (Leica DMi8, Wetzlar, Germany) equipped with a digital camera. IOD for fluorescence intensity was quantitatively analyzed by Image-Pro Plus 6.0 software as described above.

2.8. Western blot analysis

Western blot analysis was performed in three independent experiments, as described previously (Chen et al., 2008). Briefly, the indicated cells, after treatments, were washed with cold PBS, and then on ice, lysed in the radioimmunoprecipitation assay buffer. After that, lysates containing equivalent amounts of protein were separated on 7–12% SDS–polyacrylamide gel and transferred to polyvinylidene difluoride membranes (Millipore, Bedford, MA, USA). Membranes were incubated with PBS containing 0.05% Tween 20 and 5% nonfat dry milk to block nonspecific binding, and then with primary antibodies against phosphorylated Akt (p-Akt) (Ser473), p-Akt (Thr308), p-glycogen synthase kinase3β (GSK3β)(Ser9), cleaved-caspase-3, poly (ADP-ribose) polymerase (PARP) (Cell Signaling Technology, Danvers, MA, USA), Akt, GSK3β, LC3, SQSTM1/p62, β-tubulin (Sciben Biotech Company), HA (Sigma) overnight at 4 °C, respectively, followed by incubating with appropriate secondary antibodies including horseradish peroxidase-coupled goat anti-rabbit IgG, goat anti-mouse IgG, or rabbit anti-goat IgG (Pierce, Rockford, IL, USA) overnight at 4 °C. Immunoreactive bands were visualized by using enhanced chemiluminescence solution (Sciben Biotech Company). The blots for detected proteins were semi-quantified using NIH Image J software (National Institutes of Health, Bethesda, MD, USA).

2.9. Statistical analysis

Results were expressed as means ± standard error of the mean (SEM). Student's *t*-test for non-paired replicates was used to identify statistically significant differences between treatment means. Group variability and interaction were compared using either one-way or two-way ANOVA followed by Bonferroni's post-tests to compare replicate means. *p*-value of < 0.05 was considered significant.

3. Results

3.1. Mad induces apoptosis in skeletal myoblast cells

C2C12 and L6 cells, the two skeletal myoblast cell lines were chosen as models to study how Mad induces apoptosis of skeletal muscle cells. To determine the effect of Mad on the cell apoptosis, we first evaluated the cell nuclear fragmentation and condensation, a hallmark of apoptosis (Hao et al., 2013), using DAPI staining, and concurrently examined DNA strand breaks in the cells by TUNEL staining. As shown in Fig. 1A and B, treatment with Mad for 24 h obviously elicited a concentration-dependent increase of nuclear fragmentation and condensation (arrows) in C2C12 and L6 cells. Consistently, Mad substantially increased the number of TUNEL-positive cells with fragmented DNA (in green), compared to the vehicle control (Fig. 1 A and B). Subsequently, we analyzed the cleavages of caspase-3 and PARP in the cells. The results revealed that Mad resulted in robust cleavages of caspase-3 and PARP in a concentration-dependent manner in the cells (Fig. 1C and D). In line with the increased level of cleaved-caspase-3, Mad profoundly evoked the activation of caspases-3/7 in the cells as well (Fig. 1E). These findings clearly indicate that Mad induces caspase-dependent apoptosis in skeletal myoblast cells.

3.2. Mad triggers an increase in autophagosomes with a concomitant elevation of LC3-II and p62 in skeletal myoblast cells

Autophagy, a lysosomal degradation pathway, is essential for cell survival, differentiation, and homeostasis (Levine and Kroemer, 2008). Numerous studies have documented that autophagic dysfunction is associated with cell apoptosis (Levine and Kroemer, 2008; Mizushima et al., 2008). Recently, we have shown that Mad-induced apoptosis is related to increased autophagosomes, LC3-II and p62 in H9c2 cells (Chen et al., 2018). Here, we also observed that Mad treatment substantially elevated the protein levels of LC3-II and p62 in a concentration-dependent manner in C2C12 and L6 cells (Fig. 2 A and B), as detected by Western blot analysis. Subsequently, the autofluorescent drug MDC, a specific autophagolysosome marker (Biederbick et al., 1995; Munafo and Colombo, 2001), was utilized. We revealed that the accumulation of MDC was significantly induced by Mad dose-dependently in C2C12 and L6 cells, as evidenced by the fluorescence intensity (in green) and quantification based on the incorporation of MDC (Fig. 2C and D). To corroborate the finding, we extended the studies by analyzing autophagic vacuoles with GFP-LC3 localization. The results

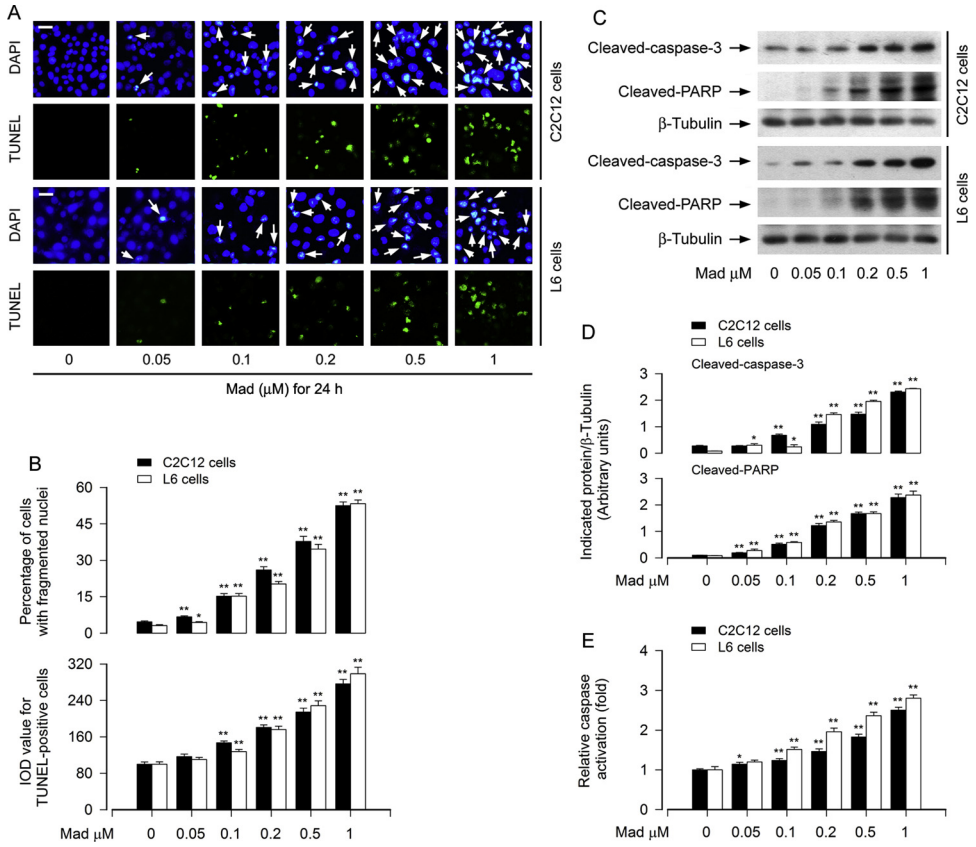

Fig. 1. Mad induces apoptosis in skeletal myoblast cells in a concentration-dependent manner. C2C12 and L6 cells were treated with Mad (0–1 μM) for 24 h. (A) Apoptotic cells were evaluated by nuclear fragmentation and condensation (arrows) using DAPI staining (upper panel) and concurrently by *in situ* detection of fragmented DNA (in green) using TUNEL staining (lower panel). Scale bar: 20 μm. (B) The percentage of cells with fragmented nuclei and the number of TUNEL-positive cells were quantified. (C) Total cell lysates were subjected to Western blotting using indicated antibodies. The blots were probed for β-tubulin as a loading control. Similar results were observed in at least three independent experiments. (D) The blots for cleaved-caspase-3 and cleaved-PARP were semi-quantified. (E) Caspase-3/7 activities were detected using Caspase-3/7 Assay Kit. Results are presented as mean ± SEM ($n = 3$–5). $^{*}p < 0.05$, $^{**}p < 0.01$, difference with control group.

showed that when C2C12 and L6 cells, infected with Ad-GFP-LC3, were treated with Mad (0–1 μM) for 24 h, the number of LC3 puncta per cell markedly increased compared to that of the vehicle-treated cells in a concentration-dependent fashion (Fig. 2E and F). These data are consistent with the finding that Mad induced cell apoptosis (Fig. 1). Taken together, the above results indicate that Mad triggers an increase in autophagosomes with a concomitant elevation of LC3-II and p62 in skeletal myoblast cells, suggesting that Mad might impair autophagic flux, leading to expansion of abnormal autophagsomes and subsequent cell apoptosis.

3.3. Mad impairs autophagic flux contributing to accumulated autophagosomes-dependent apoptosis in skeletal myoblast cells

Multiple data have demonstrated that increase of autophagosomes may be either indicative of autophagy induction or inhibitive of autophagosome clearance (Lau et al., 2013). Autophagic flux impairment has been implicated as a mechanism for promotion of cell death with autophagosome accumulation (Gonzalez-Rodriguez et al., 2014; Ma et al., 2012; Qiu et al., 2014; Yi et al., 2018). Next, we asked whether Mad-induced autophagosome accumulation was due to autophagic flux impairment, thus leading to apoptosis in skeletal myoblast cells. Firstly, we measured autophagic flux in C2C12 and L6 cells infected with adenovirus expressing mCherry-GFP tandem-tagged-LC3 (Ad-mCherry-GFP-LC3). As shown in Fig. 3A (merged), the cells in the vehicle (0 μM Mad)-treated group exhibited only red puncta (autolysosomes), whereas the cells in the Mad (0.5 and 1 μM)-treated groups had both yellow (autophagosomes) and red puncta (autolysosomes). When mCherry-GFP-LC3 was overexpressed in the cells treated with Mad (0.5 and 1 μM), we detected more autophagosomes ($GFP^+/mCherry^+$-LC3) than autolysosomes ($GFP^-/mCherry^+$-LC3) (Fig. 3A). Concentration-dependent increase of $GFP^+/mCherry^+$-LC3 (yellow) puncta (Fig. 3B) per cell in response to Mad was quantified. These results point out that Mad inhibits autophagic flux, resulting in accumulation of autophagosomes in skeletal myoblast cells.

To demonstrate the role of impaired autophagic flux in Mad-induced apoptosis in skeletal myoblast cells, C2C12 and L6 cells were subjected to pretreatment with/without CQ (5 μM), an agent capable of effectively inhibiting the fusion of autophagosomes and lysosomes (Klionsky et al., 2008), for 1 h, followed by exposure to Mad (0.5 and 1 μM) for 24 h. As shown in Fig. 3C-G, treatment with CQ substantially potentiated the basic and Mad-enhanced LC3-II, p62, and cleaved-caspase-3 levels (Fig. 3C and D), autophagosome formation (Fig. 3E and F) and cell apoptosis (Fig. 3G). The results suggest that Mad treatment causes accumulation of autophagosomes and consequential cell apoptosis by impairing autophagic flux in skeletal myoblast cells.

Rapamycin, a well-known inducer of autophagy, has been reported to stimulate autophagy with enhanced autophagic flux and accelerate the fusion of autophagosomes and lysosomes in various cells (Ma et al., 2012; Qiu et al., 2014; Yi et al., 2018; Zhang et al., 2015). To corroborate the association of impaired autophagic flux with accumulated autophagosomes-dependent cell apoptosis, C2C12 and L6 cells were pretreated with/without rapamycin (0.2 μg /ml) for 24 h and then exposed to Mad (0.5 and 1 μM) for 24 h. As expected, treatment with rapamycin alone increased LC3-II but reduced p62 protein level, compared with the vehicle treatment (Fig. 4A and B), indicating intact autophagic flux. Of importance, pretreatment with rapamycin obviously mitigated Mad-increased LC3-II protein level and especially profoundly attenuated Mad-induced p62 accumulation, implying a recovery of the authophagic flux (Fig. 4A and B). This effect was in parallel to the decreased numbers of GFP-p62 and GFP-LC3 puncta per cell in Mad-treated cells in the presence of rapamycin, although there was an obviously increased GFP-LC3 puncta per cell pretreated with rapamycin alone, as visualized by images and quantification using GFP-p62 and GFP-LC3 assay, respectively (Fig. 4C–E). Additionally, as predicted, we also observed that rapamycin alleviated cleaved caspase-3 (Fig. 4A and B) and apoptosis (Fig. 4F) in the cells exposed to Mad. Collectively, our findings support the concept that Mad impairs

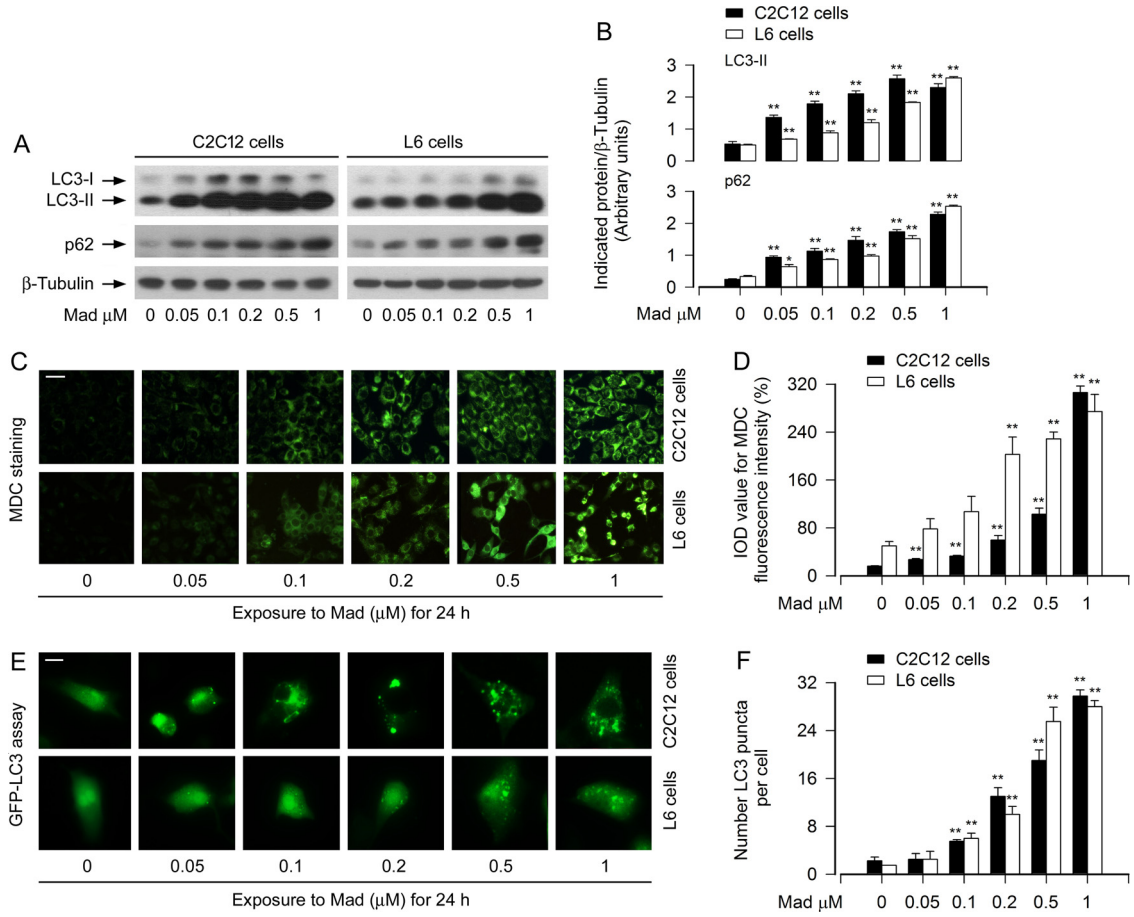

Fig. 2. Mad triggers an increase in autophagosomes with a concomitant elevation of LC3-II and p62 in skeletal myoblast cells. C2C12 and L6 cells, or C2C12 and L6 cells infected with Ad-GFP-LC3, respectively, were treated with Mad (0–1 μM) for 24 h. (A) Total cell lysates were subjected to Western blotting using indicated antibodies. The blots were probed for β-tubulin as a loading control. Similar results were observed in at least three independent experiments. (B) The blots for LC3-II and p62 were semi-quantified. (C and D) The cells were labeled using a specific autophagolysosome marker MDC staining and then the fluorescence intensity (in green) for MDC-labeled vacuoles was imaged (C) and quantified (D) as described in Materials and Methods. Scale bar: 20 μm. (E and F) Shown are representative GFP-LC3 fluorescence images (in green) (E) and quantified number for GFP-LC3 puncta (F) in the cells. Scale bar: 2 μm. Results are presented as mean ± SEM (n = 3–5). $^{*}p < 0.05$, $^{**}p < 0.01$, difference with control group.

autophagic flux contributing to accumulated autophagosomes-dependent apoptosis in skeletal myoblast cells.

3.4. Mad inactivation of Akt impairs autophagic flux leading to accumulated autophagosomes-dependent apoptosis in skeletal myoblast cells

It is known that Akt plays a critical role in cell survival (Degtyarev et al., 2008; Dudek et al., 1997). Akt can mediate autophagy, and its inactivation is closely related to dysfunction of autophagic flux and cell death in various cells (Arico et al., 2001; Bruntz et al., 2014; Degtyarev et al., 2008; Kuo et al., 2006; Rodriguez-Hernandez et al., 2018). Therefore, we hypothesized that Akt signaling may be involved in Mad-impaired autophagic flux, leading to accumulated autophagosomes-dependent apoptosis in skeletal myoblast cells. To test this hypothesis, firstly, we examined the phosphorylation status of Akt and its substrate GSK3β in C2C12 and L6 cells exposed to Mad. The results showed that Mad inhibited the phosphorylation of Akt (Thr308 and Ser473) and GSK3β (Ser9) in the cells dose-dependently (Fig. 5A and B), indicating that Mad indeed inactivates the Akt pathway. Next, C2C12 and L6 cells were pretreated with/without Akt inhibitor X (10 μM) for 2 h, and then exposed to Mad (0.5 and 1 μM) for 24 h. We found that pretreatment with Akt inhibitor X profoundly reduced the basal p-Akt and p-GSK3β and further potentiated Mad's inhibitory effects on p-Akt and p-GSK3β (Fig. 5C and D). Accordingly, Akt inhibitor X not only further enhanced the basal and Mad-induced LC3-II and p62 levels (Fig. 5C and D), but also increased the number of GFP-LC3 puncta (Fig. 5E), reflecting a more severe deterioration of autophagic flux in Mad-treated cells in the presence of Akt inhibitor X. In addition, Akt inhibitor X also showed more potent enhancement of Mad-elicited cleaved-caspase-3 (Fig. 5C and D), cell viability reduction (Fig. 5F) and apoptosis (Fig. 5G). These data suggest that Mad inactivation of Akt links impaired autophagic flux to accumulated autophagosomes-dependent apoptosis in skeletal myoblast cells.

3.5. Ectopic expression of constitutively active Akt rescues Mad-impaired autophagic flux from accumulated autophagosomes-dependent apoptosis in skeletal myoblast cells

To verify the above finding, C2C12 cells, infected with recombinant adenovirus encoding HA-tagged constitutively active Akt (Ad-myr-Akt) or LacZ (Ad-LacZ) (as control), were treated with/without Mad (0.5 or 1 μM) for 24 h. As expected, infection with Ad-myr-Akt, but not Ad-LacZ, evoked expression of high levels of HA-tagged Akt mutant in the cells (Fig. 6A and B). The basal and/or Mad-inhibited Akt and GSK3β phosphorylation levels were significantly elevated by the infection with Ad-myr-Akt, compared to the control infection with Ad-LacZ (Fig. 6A and B). Of note, overexpression of myr-Akt dramatically attenuated Mad-induced increase of LC3-II and p62 as well as activation of caspase-3 (Fig. 6A and B). Consistently, we also observed that the number of LC3 puncta was reduced in Mad-treated C2C12 cells infected with Ad-

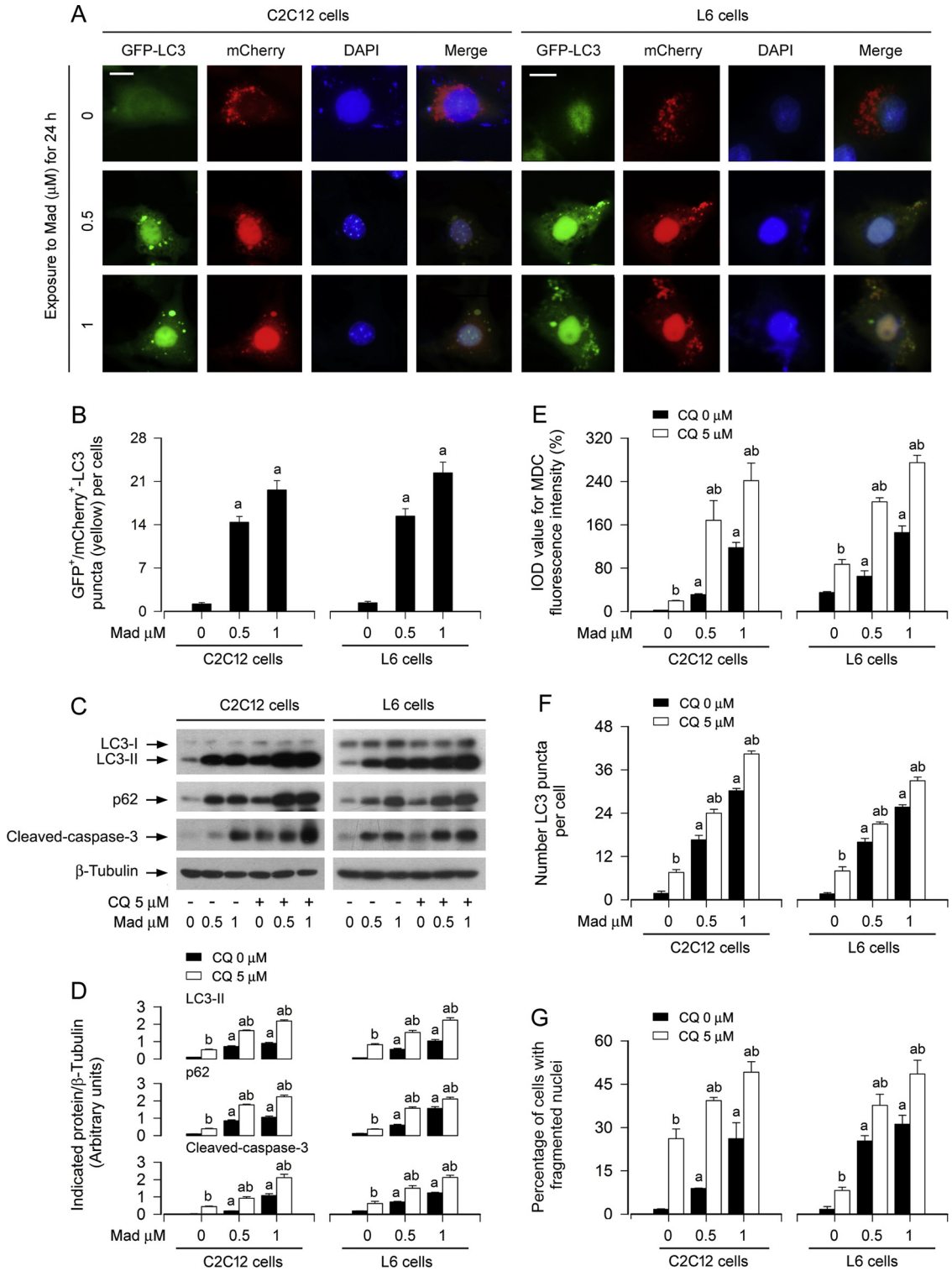

Fig. 3. Mad elicits impaired autophagic flux leading to autophagosome-dependent apoptosis in skeletal myoblast cells. C2C12 and L6 cells, or C2C12 and L6 cells infected with Ad-mCherry-GFP-LC3 or Ad-GFP-LC3, respectively, were treated with/ without Mad (0.5 and 1 μM) for 24 h, or pretreated with/without CQ (5 μM) for 1 h and then treated with/without Mad (0.5 and 1 μM) for 24 h. (A) Co-localization of both GFP and mCherry fluorescence for $GFP^+/mCherry^+$-LC3 (yellow) puncta was shown in the cells. Scale bar: 2 μm. (B) $GFP^+/mCherry^+$-LC3 puncta per cell were quantified. (C) Total cell lysates were subjected to Western blotting using indicated antibodies. The blots were probed for β-tubulin as a loading control. Similar results were observed in at least three independent experiments. (D) The blots for LC3-II, p62, and cleaved-caspase-3 were semi-quantified. (E) The fluorescence intensity for MDC-labeled vacuoles in the cells was quantified. (F) The number of GFP-LC3 punctate structures per cell was counted and calculated. (G) Apoptotic cells were evaluated by nuclear fragmentation and condensation using DAPI staining. Results are presented as mean ± SEM (n = 3–5). $^{a}p < 0.05$, difference with control group; $^{b}p < 0.05$, – CQ group versus + CQ group.

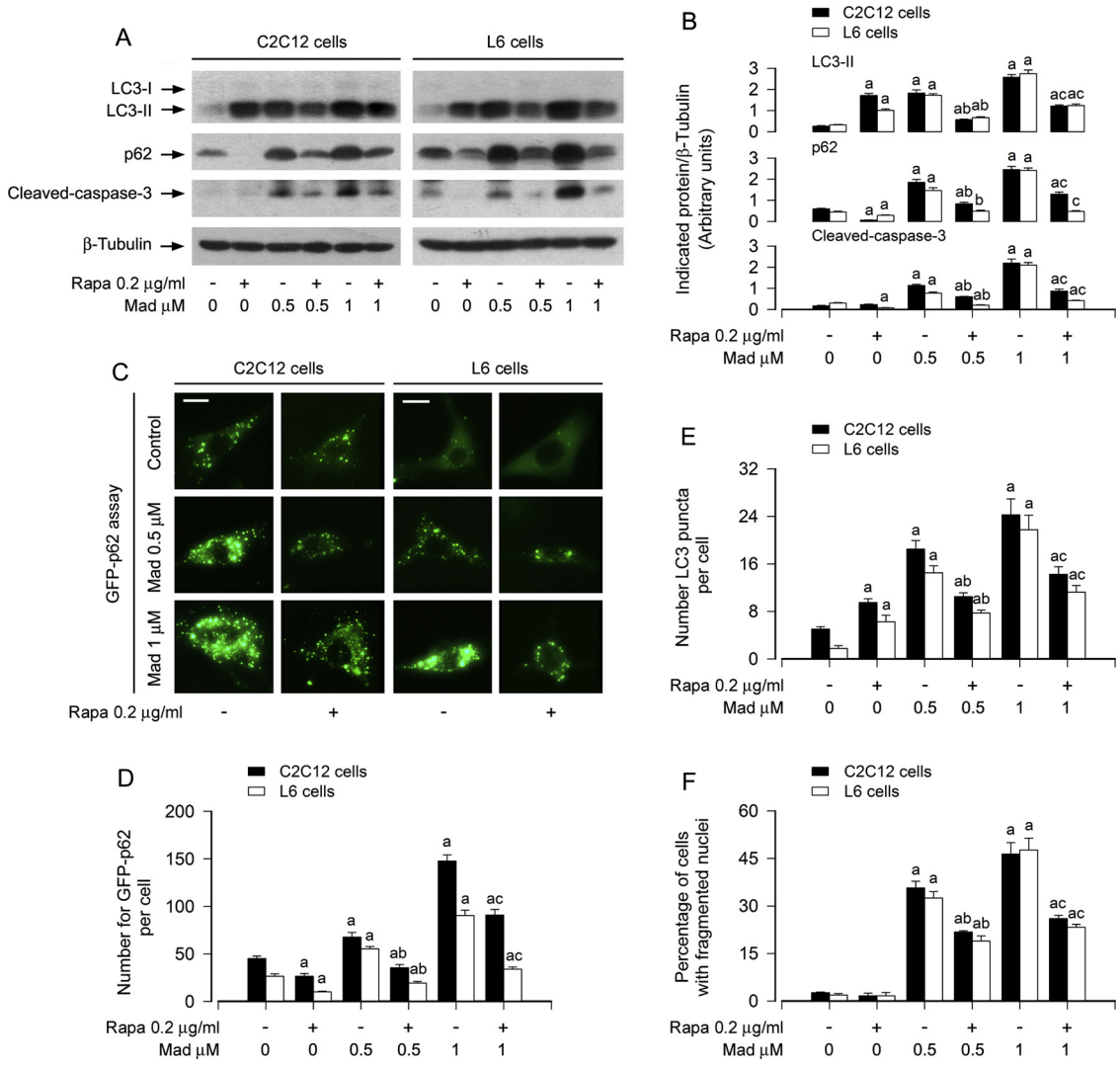

Fig. 4. Rapamycin rescues Mad-impaired autophagic flux from accumulated autophagosomes-dependent apoptosis in skeletal myoblast cells. C2C12 and L6 cells, or C2C12 and L6 cells infected with Ad-GFP-p62 or Ad-GFP-LC3, respectively, were pretreated with/without rapamycin (Rapa, 0.2 μg/ml) for 24 h and then treated with/without Mad (0.5 and 1 μM) for 24 h. (A) Total cell lysates were subjected to Western blotting using indicated antibodies. The blots were probed for β-tubulin as a loading control. Similar results were observed in at least three independent experiments. (B) The blots for LC3-II, p62, and cleaved-caspase-3 were semi-quantified. (C and D) Shown were representative GFP-p62 fluorescence images (in green) (C) and quantified number for GFP-p62 (D) in the cells. Scale bar: 2 μm. (E) The number of GFP-LC3 punctate structures per cell was counted and calculated. (F) Apoptotic cells were evaluated by nuclear fragmentation and condensation using DAPI staining. Results are presented as mean ± SEM (n = 3–5). $^{a}p < 0.05$, difference with control group; $^{b}p < 0.05$, difference with 0.5 μM Mad group; $^{c}p < 0.05$, difference with 1 μM Mad group.

myr-Akt (Fig. 6C and D). Using MTS assay and DAPI staining, we revealed that ectopic expression of myr-Akt partially prevented Mad-induced cell viability reduction (Fig. 6E) and apoptosis (Fig. 6F). In addition, using mCherry-GFP tandem-tagged LC3 assay, we found that there existed fewer GFP^{+}/$mCherry^{+}$-LC3 (yellow) puncta in the cells expressing myr-Akt than in the cells expressing LacZ (as control) (Fig. 6G and H). These findings exhibit that Mad inactivation of Akt plays an essential role in impaired autophagic flux, accumulated autophagosomes and apoptotic cell death in skeletal myoblast cells.

4. Discussion

It has been widely reported that Mad, a polyether ionophore antibiotic, is extensively used to prevent chicken and turkey coccidiosis (Dorne et al., 2013; Jayashree and Singhi, 2011; Sharma et al., 2005; Shimshoni et al., 2014; Singh and Gupta, 2003). Mad can be absorbed through the digestive tract and metabolized in the liver and kidney, finally excreted in urine and feces (Wang et al., 2008). In addition, Mad is mainly excreted as a prototype drug and stable in excrement for 3 days, which makes it possible to contaminate soil and water, and finally get into the food chain (Brown and Rajan, 1986; Singh and Gupta, 2003). Comparing to other polyether antibiotics, Mad is more toxic to mice and rats (Oehme and Pickrell, 1999). There have been a number of reports of Mad poisoning, mainly on skeletal muscle and myocardial lesions (Dorne et al., 2013; Jayashree and Singhi, 2011; Sharma et al., 2005; Shimshoni et al., 2014), but little is known about its toxic mechanism in the cells. Recently, our group has shown that Mad evokes increases of autophagosomes, accumulation of LC3-II and p62, contributing to apoptosis in H9c2 cells (Chen et al., 2018). In the current study, we also found that Mad-induced apoptosis was associated with accumulation of autophagosomes with a concomitant elevation of LC3-II and p62 in skeletal myoblast cells. Further, we noticed that Mad inactivation of Akt impaired autophagic flux, resulting in accumulated autophagosomes-dependent cell apoptosis.

Autophagy is a highly conserved lysosomal degradation process that is required for cells to maintain homeostasis (Mizushima et al., 2008). It

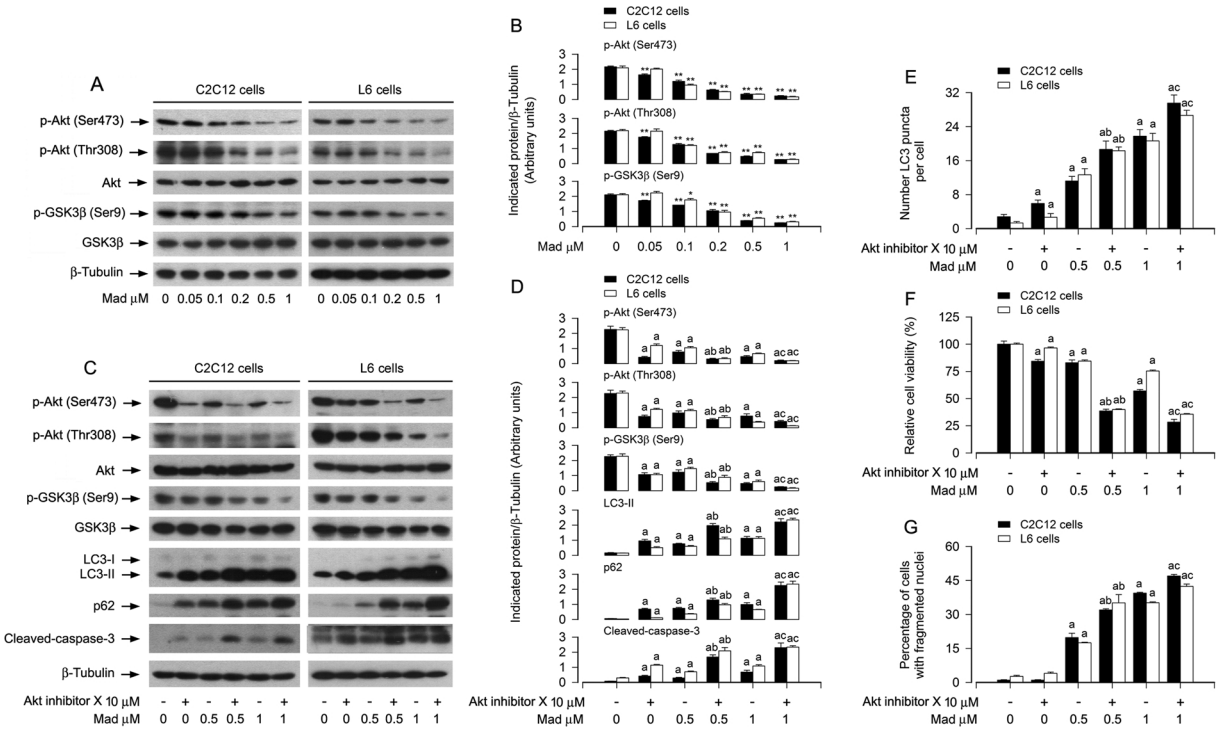

Fig. 5. Mad inactivation of Akt links impaired autophagic flux to accumulated autophagosomes-dependent apoptosis in skeletal myoblast cells. C2C12 and L6 cells, or C2C12 and L6 cells infected with Ad-GFP-LC3, respectively, were treated with Mad (0–1 μM) for 24 h, or pretreated with/without Akt inhibitor X (10 μM) for 2 h and then treated with/without Mad (0.5 and 1 μM) for 24 h. (A and C) Total cell lysates were subjected to Western blotting using indicated antibodies. The blots were probed for β-tubulin as a loading control. Similar results were observed in at least three independent experiments. (B and D) The blots for p-Akt (Ser473), p-Akt (Thr308), p-GSK3β (Ser9), LC3-II, p62 and cleaved-caspase-3 were semi-quantified. (E) The number of GFP-LC3 punctate structures per cell was counted and calculated. (F) The cell viability was determined by the MTS assay. (G) Apoptotic cells were evaluated by nuclear fragmentation and condensation using DAPI staining. Results are presented as mean ± SEM (n = 3–5). $^{a}p < 0.05$, difference with control group; $^{b}p < 0.05$, difference with 0.5 μM Mad group; $^{c}p < 0.05$, difference with 1 μM Mad group.

is well-known that the occurrence of autophagy is a double-edged sword for the physiological activity of cells (Mizushima et al., 2008; Zhang et al., 2016). Autophagosomes that failed to fuse with lysosomes might result in autophagosome accumulation and subsequent cell death (Button and Luo, 2017). The level of conversion of LC3-I to LC3-II, an indicator for autophagic activity, correlates with the number of autophagosomes formed (Mizushima et al., 2010). The p62 protein is selectively incorporated into autophagosomes through direct binding to LC3-II and efficiently degraded in the autolysosome. Accordingly, the total cellular protein level of p62 is negatively correlated with autophagic flux (Mizushima et al., 2010). Accumulation of LC3-II and autophagosomes, an event previously interpreted as induction of autophagy, is in fact a consequence of a blocked autophagic flux (Gonzalez-Rodriguez et al., 2014). The combination of elevated p62 and punctuate LC3-II could be reflecting an inhibition of autophagosome degradation (Gonzalez-Rodriguez et al., 2014). In the current study, we observed that Mad-induced apoptosis was associated with increase of autophagosomes in skeletal myoblast (C2C12 and L6) cells (Figs. 1 and 2). The results from Western blot analysis revealed that the protein levels of both LC3-II and p62 were significantly higher in Mad-treated C2C12 and L6 cells (Fig. 2E and F). In another word, accumulation of p62 was paralleled to an increase in the LC3-II, hinting that accumulation of autophagosomes by Mad is a secondary effect of the impaired autophagic flux. Similar evidence was gained when autophagic flux was evaluated using mCherry-GFP-LC3 assay, which can generate a LC3 construct tandem tagged with mCherry and GFP probes (Ma et al., 2012). In line with the immunoblotting results, C2C12 and L6 cells treated with Mad exhibited a decline in autophagic flux, as shown by the increase in the number of yellow puncta (autophagosomes) without the concomitant increase in the number of red LC3 puncta (autolysosomes) per cell. Taken together, these results support the notion that Mad may inhibit the fusion of autophagosomes with lysosomes and thus impair autophagic flux in the myoblast cells.

In autophagy, the lysosome is the only way to degrade cargos, so dysfunction of lysosomes elicits serious impairment of autophagic flux (Qiu et al., 2014). CQ is an alkalizing agent that neutralizes the pH of lysosomes and destroys the function of lysosomes, thereby inhibiting the fusion of autophagosomes with lysosomes or degradation of autophagosomes (Klionsky et al., 2008; Mizushima et al., 2010; Wu et al., 2010). To further confirm the relationship of Mad-impaired autophagic flux to myoblast cell apoptosis, we extended our studies using CQ. As expected, addition of CQ potentiated the basic and Mad-enhanced LC3-II and p62 levels, autophagosome accumulation and apoptosis in C2C12 and L6 cells (Fig. 3). Rapamycin, a known autophagy inducer, has been shown to increase autophagy flux and accelerate autophagosome-lysosome fusion (Ma et al., 2012; Qiu et al., 2014; Yi et al., 2018; Zhang et al., 2015). In this study, we also demonstrated that pretreatment with rapamycin alleviated the above events in the cells exposed to Mad (Fig. 4), implying that rapamycin plays a key role in recovering the autophagic flux. This is consistent with the observation that pretreatment with rapamycin was able to rescue cells from apoptosis induced by Mad. Collectively, these findings further highlight that Mad causes accumulation of autophagosome-bound LC3-II and p62, thereby leading to cell apoptosis via impairment of autophagic flux in skeletal myoblast cells. A new question that arises from the current work is whether impairment of autophagic flux is a key mechanism of Mad-induced myoblast cell apoptosis. More importantly, elucidation of the origin of dysfunctional autophagic processes may help design new therapeutic approaches to prevent Mad-induced myotoxicity, such as rhabdomyolysis and skeletal muscle degeneration.

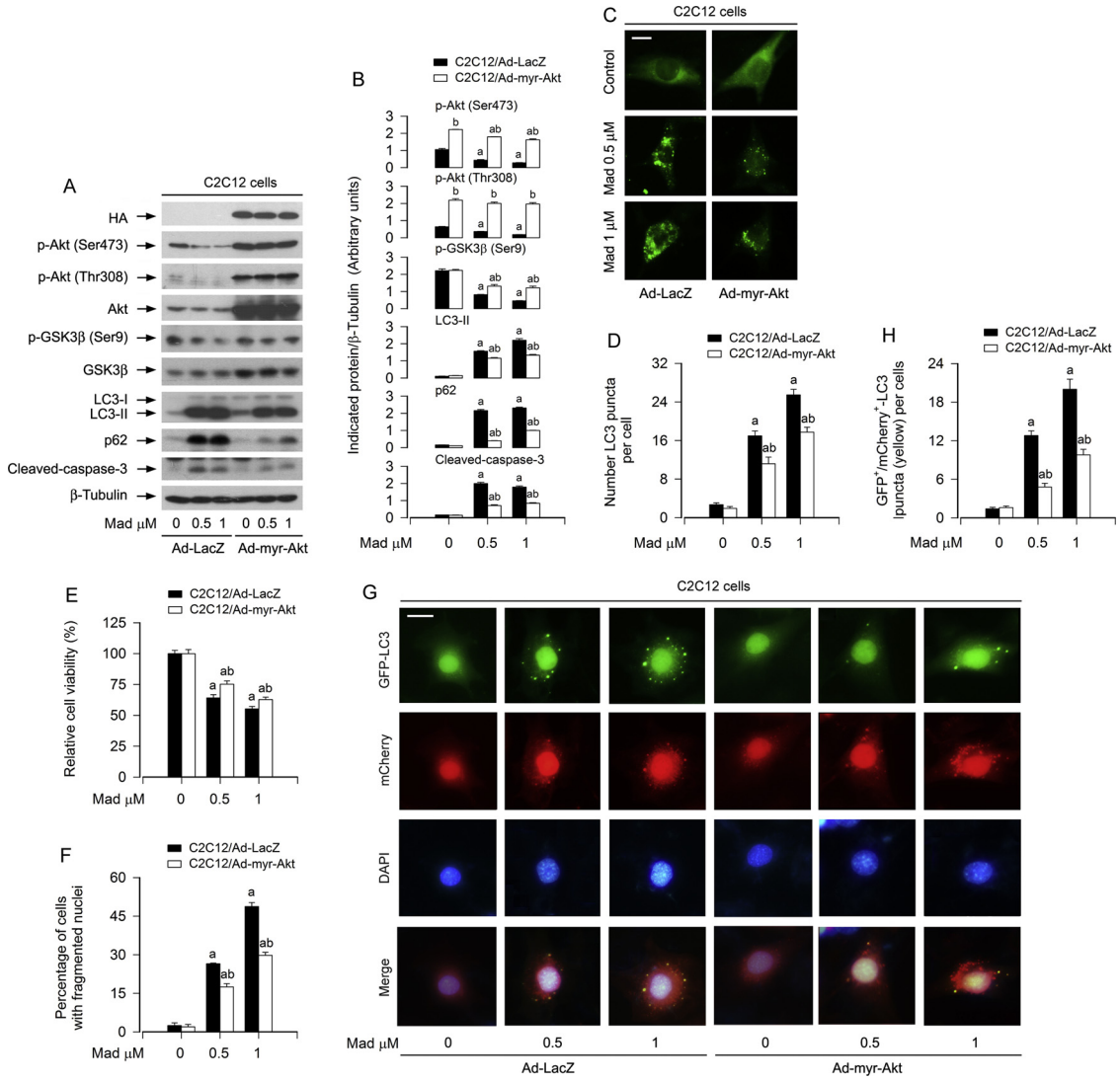

Fig. 6. Ectopic expression of constitutively active Akt prevents Mad-impaired autophagic flux from accumulated autophagosomes-dependent apoptosis in skeletal myoblast cells. C2C12 cells infected with Ad-myr-Akt, Ad-LacZ, and/or Ad-GFP-LC3, respectively, were treated with/without Mad (0.5 or 1 μM) for 24 h. (A) Total cell lysates were subjected to Western blotting using indicated antibodies. The blots were probed for β-tubulin as a loading control. Similar results were observed in at least three independent experiments. (B) The blots for p-Akt (Ser473), p-Akt (Thr308), p-GSK3β (Ser9), LC3-II, p62 and cleaved-caspase-3 were semi-quantified. (C and D) Shown were representative GFP-LC3 fluorescence images (in green) (C) and quantified number for GFP-LC3 puncta (D) in the cells. Scale bar: 2 μm. (E) The cell viability was determined by the MTS assay. (F) Apoptotic cells were evaluated by nuclear fragmentation and condensation using DAPI staining. (G) Co-localization of both GFP and mCherry fluorescence for $GFP^+/mCherry^+$-LC3 (yellow) puncta was shown in the cells. Scale bar: 2 μm. (H) $GFP^+/mCherry^+$-LC3 puncta per cell were quantified. Results are presented as mean ± SEM (n = 3–5). $^a p < 0.05$, difference with control group; $^b p < 0.05$, Ad-LacZ group versus Ad-myr-Akt group.

In this study, we also reveal an underlying mechanism that governs impairment of autophagic flux in Mad-induced myoblast cells. Akt is an important regulator of cell survival (Degtyarev et al., 2008; Dudek et al., 1997). Recently, Akt is also considered to be a"rogue"kinase in regulating the association of autophagy with apoptosis in various cells (Bruntz et al., 2014; Degtyarev et al., 2008; Rodriguez-Hernandez et al., 2018). Especially, Akt deactivation acts as an essential factor for autophagic process (Arico et al., 2001; Bruntz et al., 2014; Degtyarev et al., 2008; Kuo et al., 2006). For example, Akt inhibition blocks autophagic flux leading to cell viability reduction and death in glioblastoma cells (Bruntz et al., 2014) and in liver cancer cells (Rodriguez-Hernandez et al., 2018). In this study, we demonstrated that Mad evoked an obvious dose-dependent inactivation of Akt pathway. Inhibition of Akt with inhibitor X strengthened the basal or Mad-induced decreases of phosphorylated Akt and GSK3β, increases of LC3-II and p62 levels, autophagosome formation and cell apoptosis (Fig. 5), whereas expression of constitutively active Akt rendered resistance to the events (Fig. 6). Hence, our data support the idea that Mad inactivation of Akt impairs autophagic flux, leading to accumulation of autophagosomes, which promotes apoptosis in skeletal myoblast cells. Further research is needed to elucidate how Mad inactivates Akt.

In summary, we have identified that Mad inactivates Akt, which impairs autophagic flux, thereby leading to accumulated autophagosomes-dependent cell apoptosis (Fig. 7). Our data underscore that manipulation of Akt activity to improve autophagic flux is a promising strategy against Mad-induced myotoxicity.

Acknowledgements

This work was supported by the grants from National Natural Science Foundation of China (Nos. 81873781, 81271416; L.C.), National Institutes of Health (CA115414; S.H.), Project for the Priority Academic Program Development of Jiangsu Higher Education Institutions of China (PAPD-14KJB180010; L.C.), and American Cancer

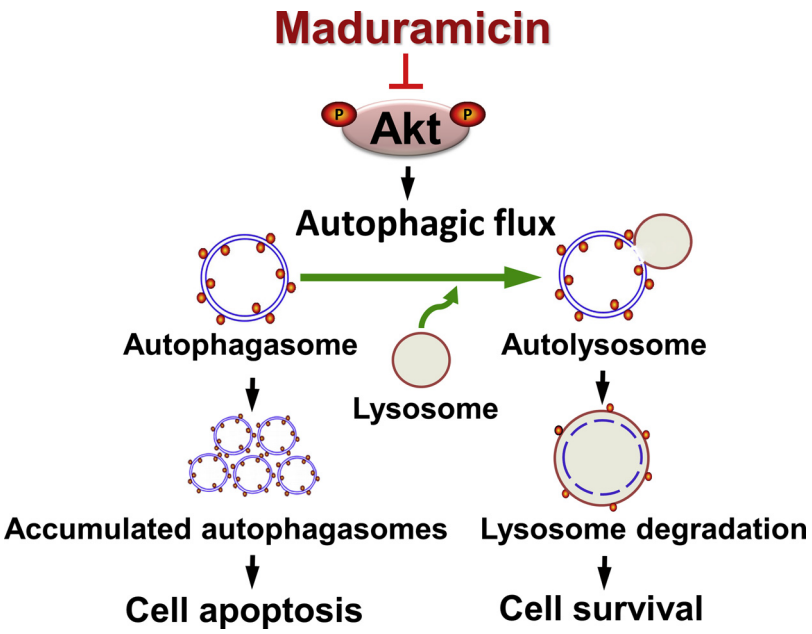

Fig. 7. Graphical model showing how Mad impairs autophagic flux contributing to skeletal myoblast cell apoptosis. Mad inactivates Akt, which impairs autophagic flux, thereby leading to accumulation of autophagosomes. Consequently, the accumulated autophagosomes promote apoptosis in skeletal myoblast cells.

Society (RSG-08-135-01-CNE; S.H.).

References

Arico, S., Petiot, A., Bauvy, C., Dubbelhuis, P.F., Meijer, A.J., Codogno, P., et al., 2001. The tumor suppressor PTEN positively regulates macroautophagy by inhibiting the phosphatidylinositol 3-kinase/protein kinase B pathway. J. Biol. Chem. 276, 35243–35246.

Biederbick, A., Kern, H.F., Elsasser, H.P., 1995. Monodansylcadaverine (MDC) is a specific in vivo marker for autophagic vacuoles. Eur. J. Cell Biol. 66, 3–14.

Brown, M.A., Rajan, S., 1986. Maduramicin: rat metabolism of a highly potent polyether anticoccidial examined by carbon-13 NMR. J. Agric. Food Chem. 34, 470–472.

Bruntz, R.C., Taylor, H.E., Lindsley, C.W., Brown, H.A., 2014. Phospholipase D2 mediates survival signaling through direct regulation of Akt in glioblastoma cells. J. Biol. Chem. 289, 600–616.

Button, R.W., Luo, S., 2017. The formation of autophagosomes during lysosomal defect: a new source of cytotoxicity. Autophagy 13, 1797–1798.

Chen, L., Liu, L., Luo, Y., Huang, S., 2008. MAPK and mTOR pathways are involved in cadmium-induced neuronal apoptosis. J. Neurochem. 105, 251–261.

Chen, X., Chen, L., Jiang, S., Huang, S., 2018. Maduramicin induces apoptosis and necrosis, and blocks autophagic flux in myocardial H9c2 cells. J. Appl. Toxicol. 38, 366–375.

Degtyarev, M., De Maziere, A., Orr, C., Lin, J., Lee, B.B., Tien, J.Y., et al., 2008. Akt inhibition promotes autophagy and sensitizes PTEN-null tumors to lysosomotropic agents. J. Cell Biol. 183, 101–116.

Deretic, V., Saitoh, T., Akira, S., 2013. Autophagy in infection, inflammation and immunity. Nat. Rev. Immunol. 13, 722–737.

Dorne, J.L., Fernandez-Cruz, M.L., Bertelsen, U., Renshaw, D.W., Peltonen, K., Anadon, A., et al., 2013. Risk assessment of coccidostatics during feed cross-contamination: animal and human health aspects. Toxicol. Appl. Pharmacol. 270, 196–208.

Dudek, H., Datta, S.R., Franke, T.F., Birnbaum, M.J., Yao, R., Cooper, G.M., et al., 1997. Regulation of neuronal survival by the serine-threonine protein kinase Akt. Science 275, 661–665.

Gonzalez-Rodriguez, A., Mayoral, R., Agra, N., Valdecantos, M.P., Pardo, V., Miquilena-Colina, M.E., et al., 2014. Impaired autophagic flux is associated with increased endoplasmic reticulum stress during the development of NAFLD. Cell Death Dis. 5, e1179.

Gutierrez-Lugo, M.T., Lotina-Hennsen, B., Farres, A., Sanchez, S., Mata, R., 1999. Phytotoxic and photosynthetic activities of maduramicin and maduramicin methyl ester. Z. Naturforsch. C 54, 325–332.

Hao, B., Cheng, S., Clancy, C.J., Nguyen, M.H., 2013. Caspofungin kills Candida albicans by causing both cellular apoptosis and necrosis. Antimicrob. Agents Chemother. 57, 326–332.

Jayashree, M., Singhi, S., 2011. Changing trends and predictors of outcome in patients with acute poisoning admitted to the intensive care. J. Trop. Pediatr. 57, 340–346.

Kabeya, Y., Mizushima, N., Ueno, T., Yamamoto, A., Kirisako, T., Noda, T., et al., 2000. LC3, a mammalian homologue of yeast Apg8p, is localized in autophagosome membranes after processing. EMBO J. 19, 5720–5728.

Klionsky, D.J., Abeliovich, H., Agostinis, P., Agrawal, D.K., Aliev, G., Askew, D.S., et al., 2008. Guidelines for the use and interpretation of assays for monitoring autophagy in higher eukaryotes. Autophagy 4, 151–175.

Kozarova, I., Macanga, J., Goldova, M., Major, P., Tkacikova, S., 2011. Detection of maduramycin residues in the tissues of chickens and pheasants by the screening test for antibiotic residues (STAR). Food Addit. Contam. Part A: Chem. Anal. Control Expo. Risk Assess. 28, 608–618.

Kuo, P.L., Hsu, Y.L., Cho, C.Y., 2006. Plumbagin induces G2-M arrest and autophagy by inhibiting the AKT/mammalian target of rapamycin pathway in breast cancer cells. Mol. Cancer Ther. 5, 3209–3221.

Levine, B., Klionsky, D.J., 2004. Development by self-digestion: molecular mechanisms and biological functions of autophagy. Dev. Cell 6, 463–477.

Levine, B., Kroemer, G., 2008. Autophagy in the pathogenesis of disease. Cell 132, 27–42.

Liu, C.M., Hermann, T.E., Downey, A., Prosser, B.L., Schildknecht, E., Palleroni, N.J., et al., 1983. Novel polyether antibiotics X-14868A, B, C, and D produced by a Nocardia. Discovery, fermentation, biological as well as ionophore properties and taxonomy of the producing culture. J. Antibiot. 36, 343–350.

Liu, L., Luo, Y., Chen, L., Shen, T., Xu, B., Chen, W., et al., 2010. Rapamycin inhibits cytoskeleton reorganization and cell motility by suppressing RhoA expression and activity. J. Biol. Chem. 285, 38362–38373.

Ma, X., Liu, H., Foyil, S.R., Godar, R.J., Weinheimer, C.J., Hill, J.A., et al., 2012. Impaired autophagosome clearance contributes to cardiomyocyte death in ischemia/reperfusion injury. Circulation 125, 3170–3181.

Mizushima, N., Klionsky, D.J., 2007. Protein turnover via autophagy: implications for metabolism. Annu. Rev. Nutr. 27, 19–40.

Mizushima, N., Levine, B., 2010. Autophagy in mammalian development and differentiation. Nat. Cell Biol. 12 (9), 823–830.

Mizushima, N., Levine, B., Cuervo, A.M., Klionsky, D.J., 2008. Autophagy fights disease through cellular self-digestion. Nature 451, 1069–1075.

Mizushima, N., Yoshimori, T., Levine, B., 2010. Methods in mammalian autophagy research. Cell 140, 313–326.

Munafo, D.B., Colombo, M.I., 2001. A novel assay to study autophagy: regulation of autophagosome vacuole size by amino acid deprivation. J. Cell. Sci. 114, 3619–3629.

Ni, H.M., Bockus, A., Wozniak, A.L., Jones, K., Weinman, S., Yin, X.M., et al., 2011. Dissecting the dynamic turnover of GFP-LC3 in the autolysosome. Autophagy 7, 188–204.

Oehme, F.W., Pickrell, J.A., 1999. An analysis of the chronic oral toxicity of polyether ionophore antibiotics in animals. Vet. Hum. Toxicol. 41, 251–257.

Olejnik, M., Jedziniak, P., Szprengier-Juszkiewicz, T., 2013. The determination of six ionophore coccidiostats in feed by liquid chromatography with postcolumn derivatisation and spectrofotometric/fluorescence detection. Sci. World J. 2013, 763402.

Olejnik, M., Szprengier-Juszkiewicz, T., Jedziniak, P., Sledzinska, E., Szymanek-Bany, I., Korycinska, B., et al., 2011. Residue control of coccidiostats in food of animal origin in Poland during 2007–2010. Food Addit. Contam. Part B: Surveill. 4, 259–267.

Qiu, W., Su, M., Xie, F., Ai, J., Ren, Y., Zhang, J., et al., 2014. Tetrandrine blocks autophagic flux and induces apoptosis via energetic impairment in cancer cells. Cell Death Dis. 5, e1123.

Rodriguez-Hernandez, M.A., Gonzalez, R., de la Rosa, A.J., Gallego, P., Ordonez, R., Navarro-Villaran, E., et al., 2018. Molecular characterization of autophagic and apoptotic signaling induced by sorafenib in liver cancer cells. J. Cell. Physiol. 234, 692–708.

Rokka, M., Eerola, S., Perttila, U., Rossow, L., Venalainen, E., Valkonen, E., et al., 2005. The residue levels of narasin in eggs of laying hens fed with unmedicated and medicated feed. Mol. Nutr. Food Res. 49, 38–42.

Sharma, N., Bhalla, A., Varma, S., Jain, S., Singh, S., 2005. Toxicity of maduramicin.

Emerg. Med. J. 22 (12), 880–882.
Shimshoni, J.A., Britzi, M., Pozzi, P.S., Edery, N., Berkowitz, A., Bouznach, A., et al., 2014. Acute maduramicin toxicosis in pregnant gilts. Food Chem. Toxicol. 68, 283–289.
Singh, T., Gupta, R.P., 2003. Clinico-haematological and mineral studies on experimental maduramicin toxicity in chickens. Vet. Parasitol. 116, 345–353.
Spisso, B.F., Pereira, M.U., Ferreira, R.G., Monteiro, M.A., da Costa, R.P., Cruz, T.A., et al., 2010. Pilot survey of hen eggs consumed in the metropolitan area of Rio de Janeiro, Brazil, for polyether ionophores, macrolides and lincosamides residues. Food Addit. Contam. Part B: Surveill. 3, 212–219.
Wang, Z.H., Zhang, S.X., Murtazina, N.R., Erernin, S.A., Shen, J.Z., 2008. Determination of the veterinary drug maduramicin in food by fluorescence polarisation immunoassay. Int. J. Food Sci. Technol. 43, 114–122.
Wu, Y.T., Tan, H.L., Shui, G., Bauvy, C., Huang, Q., Wenk, M.R., et al., 2010. Dual role of 3-methyladenine in modulation of autophagy via different temporal patterns of inhibition on class I and III phosphoinositide 3-kinase. J. Biol. Chem. 285, 10850–10861.
Yi, H., Wang, K., Du, B., He, L., Ho, H., Qiu, M., et al., 2018. Aleuritolic acid impaired autophagic flux and induced apoptosis in hepatocellular carcinoma HepG2 cells. Molecules 23 pii: E1338.
Yin, Y., Sun, G., Li, E., Kiselyov, K., Sun, D., 2017. ER stress and impaired autophagy flux in neuronal degeneration and brain injury. Ageing Res. Rev. 34, 3–14.
Zhang, X.J., Chen, S., Huang, K.X., Le, W.D., 2013. Why should autophagic flux be assessed? Acta Pharmacol. Sin. 34 (5), 595–599.
Zhang, Y., Han, Q., You, S., Cao, Y., Zhang, X., Liu, H., et al., 2015. Rapamycin promotes the autophagic degradation of oxidized low-density lipoprotein in human umbilical vein endothelial cells. J. Vasc. Res. 52, 210–219.
Zhang, Z., Miah, M., Culbreth, M., Aschner, M., 2016. Autophagy in neurodegenerative diseases and metal neurotoxicity. Neurochem. Res. 41, 409–422.